Research article

Dynamic modeling and simulation of the MUN Explorer autonomous underwater vehicle with a fuel cell system

Mohamed M. Albarghot[1,*], Mohamed T. Iqbal[2], Kevin Pope[1] and Luc Rolland[3]

[1] Department of Mechanical Engineering, Memorial University of Newfoundland, St. John's, NL, Canada

[2] Department of Electrical Engineering, Memorial University of Newfoundland, St. John's, NL, Canada

[3] School of Computing, Engineering and Physical Sciences, University of the West Scotland, Paisley, Scotland, UK

* **Correspondence:** Email: mma216@mun.ca.

Abstract: The actual power system of the MUN Explorer Autonomous Underwater Vehicles (*AUVs*) uses 11 Lithium-ion (*Li-ion*) batteries as a main energy source. The batteries are directly connected into the BLDC motor to run the MUN Explorer for the desired operating sequence. This paper presents a dynamic model of the MUN Explorer AUV including a fuel cell system to run under the same operating conditions as suggested by its manual. A PI controller was applied into the dynamic model to maintain the operating conditions such as motor speed, DC bus voltage and the load torque, due to its advantages and simplicity for tuning technique. The MUN Explorer AUV dynamic model with a fuel cell is a proposed system to increase the power capacity, it is better to use a simple controller to see the system behaviors. The simulation of the entire system dynamics model along with the proportional-integral (*PI*) controller is done in MATLAB / Simulink. The simulation results are included in the paper. The DC bus voltage is measured at 48 V, and the motor speed is 20 (rad/s), which is equivalent to 190 (rpm). The power profile of the fuel cell and battery are presented and plotted against time. The PI controller gives satisfactory results in terms of maintaining the same operating conditions of the MUN Explorer AUV with a fuel cell.

Keywords: MUN Explorer Autonomous Underwater Vehicles (*AUVs*); fuel cell; power system

Abbreviations: AUV: Autonomous Underwater Vehicle; DC: Direct current; P_b: Pressure of the tank (Pa); P_{bi}: Initial pressure of the tank (Pa); T_b: Operating temperature (K); N_{H2}: Normal hydrogen flow rate (Liter/min); V_b: Volume of the tank (m^3); T: Temperature (K); CF: Compressibility factor; V_m: Molar volume (m^3); P: Pressure (pa); H_2O: Water; H_2: Hydrogen gas; O_2: Oxygen gas; P_{H2}: Hydrogen pressure Anode side (Pa); R: Universal gas constant (J/ (mol.K); V_a: Anode's volume (m^3); H_{2in}: Hydrogen input flow rate (kg/sec); H_{2out}: Hydrogen output flow rate (kg/sec); P_{o2}: Oxygen pressure cathode side (Pa); V_c: Cathode's volume (m^3); O_{2in}: Oxygen input flow rate (kg/sec); O_{2out}: Oxygen output flow rate (kg/sec); E: Controlled voltage source (V); E_{OC}: Open circuit voltage (V); N: Number of cells; A: Tafel slope (V); i_0: Exchange current (A); T_d: Response time (sec); R_{ohm}: Internal resistance (ohm); I_{FC}: Fuel cell current (A); V_{FC}: Fuel cell voltage (V); τ: Constant time (Sec); E_{Batt}: Nonlinear voltage (V); E_0: Constant voltage(V); Exp(s): Exponential zone dynamics (V); K: Polarization constant (Ah^{-1}); i*: Low frequency current dynamics(A); i: Battery current(A); it: Extracted capacity (Ah); Q: Maximum battery capacity (Ah); A: Exponential voltage(V); B: Exponential capacity (Ah^{-1}); Ah: Ampere hour; K_m: Torque constant (V·s/rad); e_a, e_b, e_c: Back-EMF waveforms of the phases (V); i_a, i_b, i_c: Currents of each phases (A); ω_r: Motor speed (rad/s); T_e: Electromagnetic torque (N.m); B: Damping coefficient [N.m/(rad/sec)]; J: Motor shaft (kg*m^2); T_L: Mechanical torque (N.m)

1. Introduction

1.1. Background

For the design and operations of AUVs, the control system is classified as one of the most important system, especially when it comes to renewable energy system implemented on submarines where batteries, fuel cells, charging stations, and electrical loads are concerned. Management control schemes are used to deal with many issues such as nonlinearities and maintaining certain operating conditions, the number of production energy sources and load requirements [1].

Renewable energy sources, storage systems (fuel cells and batteries) as well as the energy demand of many applications such as submarines and AUV applications are essential for sustainability and the reduction of CO_2 emissions. To maximize the amount of energy generated by fuel cell and batteries, a system controller plays a significant role in generating and consuming power precisely and effectively. The energy generation should be maximized, and it should be used directly by the motors and sensors as much as possible. As far as batteries and fuel cell are concerned, we wish to reduce losses during energy transfer and conversions. Moreover, the energy consumption must be as low as possible to overcome the challenges of limited energy availability in submarines working underwater [2].

A Classical Proportional Integral (*PI*) controller is used in the dynamic model systems to control the main performance parameters such as the fuel cell power, battery state of charge (*SOC*), motor speed and *DC* bus voltages. Using a PI feedback controller does not require advanced knowledge to implement, and the tuning can be done online for better tracking. A PI controller is linked to a PWM, especially for fuel cell current control [3,4].

The MUN Explorer AUV was constructed to do mapping-type missions of underwater depths as well as survey missions. These missions require a lot of power in order to reach seabeds (i.e. 3000 meters). 11 rechargeable lithium-ion (*Li-ion*) batteries were carried by the MUN Explorer as the

main power source with a total capacity of 14.6 kWh to 17.952 kWh, and the explorer can run for 10 hours [5].

Lithium-ion (*Li-ion*) batteries have been enhanced in the last ten years, and they now have higher efficiency, higher energy and power density, and lower self-discharge when compared to other batteries such as NiCd, NiMH, and lead acid batteries. To ensure that the Li-ion battery is running at a suitable temperature and state of charge (*SOC*), a battery control system (*BMS*) must be implemented in the system [6].

In this specific case, the Brushless DC motor includes of a rotor position sensor as well as a commutation device that has a power inverter bridge and a control circuit. These features are used to accomplish the effective control performance of the motor speed as well as the motor rotations directions [7].

1.2. Literature review

Wang et al. declared that there were only several publications dealing with the power ability and the remaining capacity when it comes to the power allocation strategy. They have developed a novel distributed energy management system based on the controller area network. They were also proposed a rule-based control strategy for the distributed energy management system to remain the capacity and the power capability of the energy storage devices. Furthermore, the Bayes Monte Carlo method is used to overcome the initial bias and noises and implemented for co-estimation of the remaining capacity and power capability of the batteries and supercapacitors [8]. Wang et al. built an energy management system for automobile system for fuel cell, battery and supercapacitor hybrid source to be more efficient and manage the energy storage devices. They established an adaptive *PID* controller to regulate the oxygen excess ratio to reached to its ideal space. This controller with fast response speed, smaller steady-state error and smaller overshoot showed better traditional feedforward control in terms of transient behavior. Moreover, the battery and fuel cell as well as battery, supercapacitor and fuel cell hybrid source for portable systems applied an energy management strategy using a new finite state machine [9]. Wang et al. proposed a comparison between fuel cell, vehicle dynamics and ultracapacitor hybrid power system as well as suboptimal on-line power distribution strategies based on classical robotics and rules. They were also used the dynamic programming algorithm as a benchmark to validate the effectiveness of the suggested strategies. Furthermore, the comparison has done by the simulations and experiments under different working conditions using a semi-physical experimental platform to check the performance of the suggested power distribution approaches [10]. Wang et al. studied three different hybrid propulsion systems which are:

1. Fuel cell and lithium-ion battery structure
2. Fuel cell and supercapacitor structure, and
3. Fuel cell, lithium-ion battery, and supercapacitor structure.

Each structure has advantages as well as disadvantages, however, the fuel cell, lithium-ion battery, and supercapacitor structure overcome the problems in 1 and 2. This work was improved the power dividing strategy for hybrid propulsion systems by using multiple-grained velocity prediction. In order to reach the optimal power dividing for different power sources, the dynamic programming strategy was introduced [11].

1.3. Paper outline and contributions

This paper extends the work of the previous paper [5] to study the dynamic model of the MUN Explorer AUV in more detail by applying a PI controller to the dynamic model with the fuel cell. This controller is implemented to achieve the operating conditions such as motor speed, DC bus voltage and the load torque during the MUN Explorer's missions. Since the MUN Explore has the challenges related to space in the dry section, this dynamic model with fuel cell is used to eliminate the number of batteries inside the MUN Explorer body and help the buoyancy force. However, the implementation of PI controller is a simple approach to see the behavior of the new dynamic model with a fuel cell. More advanced controllers are proposed for a future work. This paper also consists of four sections: The first section is the introduction. Then the second section describes the MUN Explorer power system construction and components, and the third section shows the system control with a PI controller. The fourth section is the results and discussion. Finally, this paper will finish with a concluding section.

2. MUN Explorer power system construction and components

The power system of the MUN Explorer Autonomous Underwater Vehicle is designed based on the energy and power necessities for mapping underwater depths. Figure 1 illustrates the main components and the place where we can appreciate the location of the fuel cell. Table 1 shows the parameters to be implemented and achieved by using a PI controller.
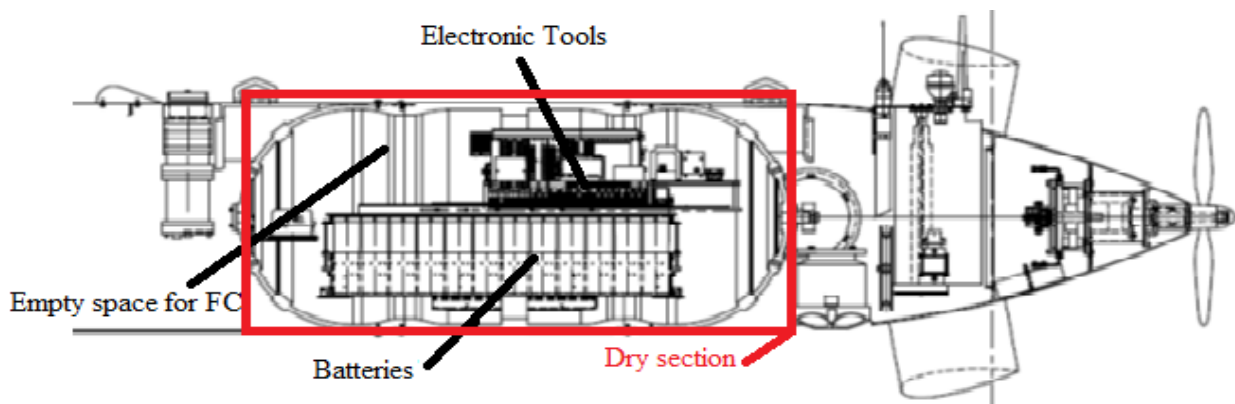

Figure 1. Side view of the MUN Explorer AUV with its components.

Table 1. The system designing parameters.

Design Parameters	Value
Fuel cell power (Min. – Max.)	(600–1200) W
Battery power ((Min. – Max.)	(350–850) W
Battery state of charge (SOC) (Min. – Max.)	(50–90) %
DC bus voltage (Min. – Max)	(47.5–50) VDC
Fuel cell current maximum	(53) A
Rotor speed	(20) rad/s

2.1. Hydrogen/Oxygen tank

The oxygen and hydrogen tanks are connected to the fuel cell to feed the required amount of oxygen and hydrogen gases. Both dynamic models of oxygen and hydrogen tanks are built based on equations (1) and (2).

$$P_b - P_{bi} = CF * \frac{N_{H2}RT_b}{M_{H2}V_b} \tag{1}$$

$$CF = \frac{PV_m}{RT} \tag{2}$$

Both are illustrated in Figures 2 and 3. All the variables in these equations are explained in the Nomenclature. The compressibility factor (CF) is equal to one when the pressure is less than 1.37 e[7] Pa (2000 psi). The CF is more than 1 when the pressure is higher than 1.37 e[7] Pa (2000 psi) at room temperature, which is well known as a function of temperature and pressure [12].

Equations 1 and 2 implemented in MATLAB / Simulink and then the pressure of each tank are measured as presented in previous work [5].
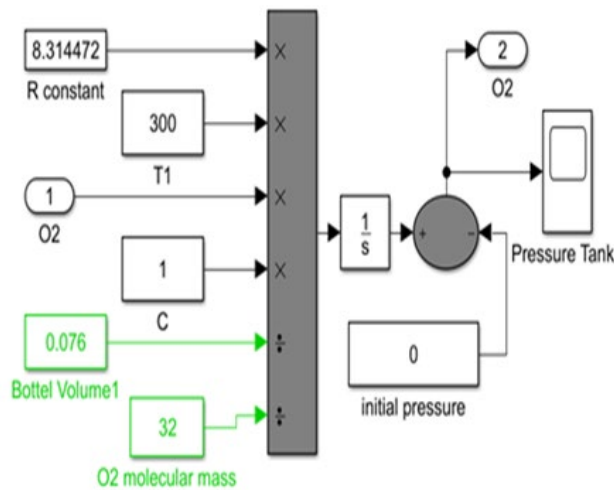
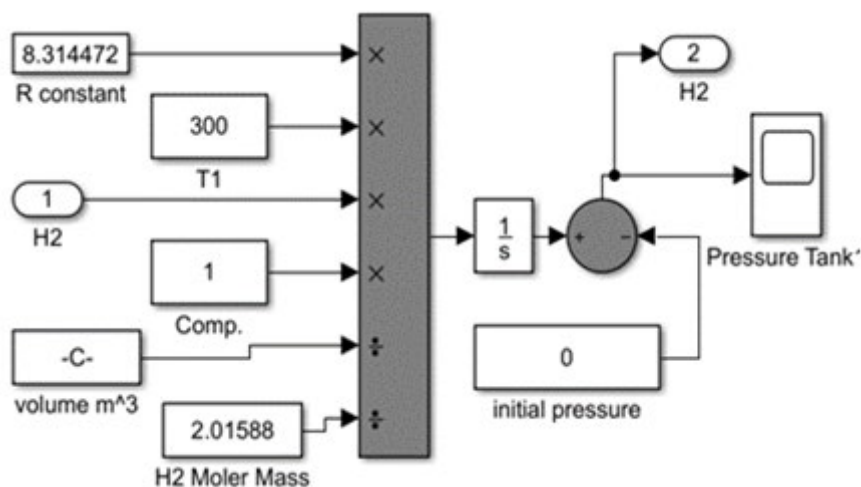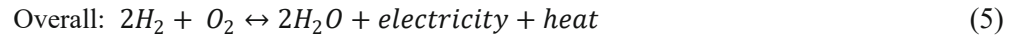**Figure 2.** Oxygen tank in MATLAB / Simulink [12].

Figure 3. Hydrogen tank in MATLAB / Simulink [12].

2.2. PEM fuel cell

A polymer electrolyte membrane (*PEM*) is an important feature of the selected fuel cell that is connected between the electrodes: the anode and cathode. The oxygen gas is injected to the cathode, whereas the hydrogen gas is injected to the anode side of the fuel cell. The overall electrochemical dynamic can be characterized by following equations [13]:

$$\text{Cathode:} O_2 + 4H^+ + 4e^- \leftrightarrow 2H_2O \tag{3}$$

$$\text{Anode:} \ \ 2H_2 \leftrightarrow 4H^+ + 4e^- \tag{4}$$

$$\text{Overall:} \ \ 2H_2 + O_2 \leftrightarrow 2H_2O + electricity + heat \tag{5}$$

The mole conservation equations can be applied for the anode and cathode in any fuel cell as follows [13]:

$$\frac{dP_{H2}}{dt} = \frac{RT}{V_a}[H_{2in} - H_{2used} - H_{2out}] \tag{6}$$

$$\frac{dP_{O2}}{dt} = \frac{RT}{V_c}[O_{2in} - O_{2used} - O_{2out}] \tag{7}$$

In MATLAB / Simulink, the dynamic model of the fuel cell stack was built using a controlled voltage source in series with a constant resistance as shown in Figure 4, and it has 42 cells [14].
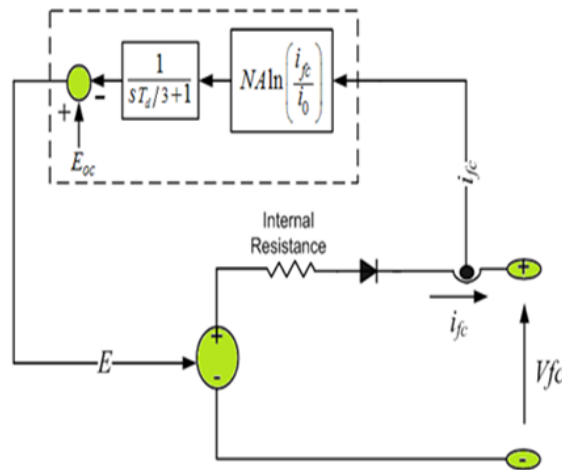

Figure 4. Fuel cell stack model [14].

The controlled voltage source (*E*) can be shown by equation (8), so that

$$E = E_{oc} - NAln\left(\frac{i_{fc}}{i_0}\right) * \frac{1}{sT_d/3+1} \tag{8}$$

$$V_{fc} = E - R_{ohm} * i_{fc} \tag{9}$$

Equations (8) and (9) show the fuel cell voltage as a function of activation losses because of the slowness of chemical reactions at the electrode surfaces and the total fuel cell voltage by taking the losses into account due to electrodes and electrolyte resistances (ohmic losses), respectively. To simulate the fuel cell at nominal conditions (pressure and temperature), a simplified model is used to represent a specific fuel cell stack and its parameters can be collected based on the polarization curve which can be found from the manufacturer datasheet. Similarly, to prevent the negative current flow into the fuel cell, a diode must be applied to the circuit [14].
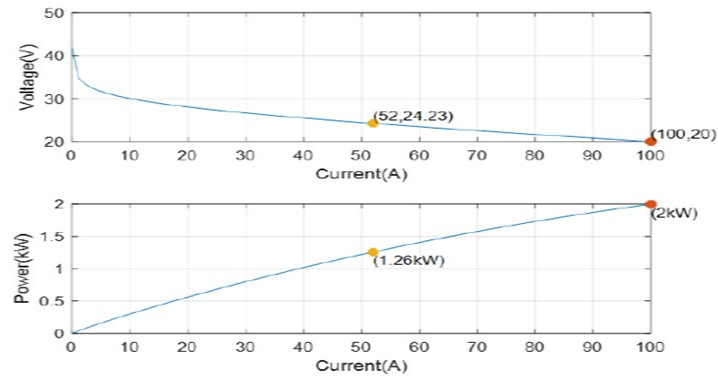
Figure 5. Polarization curves, voltage vs. current and power vs. current from simulation results [5].
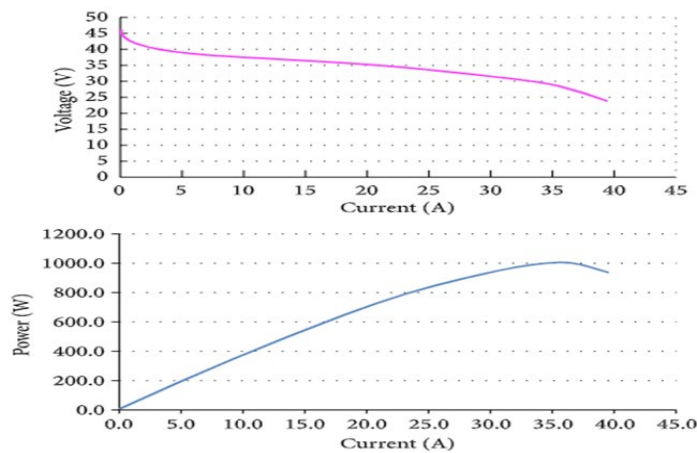

Figure 6. Polarization curves, voltage vs. current and power vs. current from data sheet results [5].

Figure 5 shows the polarization curves (*V-I and P-I*) from the simulation results, and Figure 6 illustrates the polarization curves (*V-I and P-I*) from the data sheet behavior. Both curves are almost identical from the simulations and the manufacturer's data sheet results. The fuel cell polarization curves' characteristics are defined at sea level and room ambient temperature as the baseline of operating conditions.

2.3. Lithium-Ion battery

The dynamic model of a Li-ion battery is programmed in MATLAB / Simulink based on a modified Shepherd curve-fitting model [4]. To ensure the better representation of the battery SOC effect on the battery performance, the voltage polarization term was added to the battery discharge voltage expression. The filtered battery current is applied as a replacement of the actual battery current for the polarization resistance only to improve the simulation stability. The model has two Equations for discharging and charging as follows [4]:

Discharge Model when i^* *is greater than Zero*

$$V_{batt} = E_0 - K\frac{Q}{Q-it} \cdot i^* - K \cdot \frac{Q}{Q-it} \cdot it + A \cdot exp(-B \cdot it) - R_b.I \tag{10}$$

Charge Model when i^* *is less than Zero*

$$V_{batt} = E_0 - K.\frac{Q}{it+0.1Q} \cdot i^* - K \cdot \frac{Q}{Q-it} \cdot i + A \cdot \exp(-B \cdot it) \tag{11}$$

Figure 7 demonstrates the dynamic model for a Li-ion battery in MATLAB / Simulink. From the dynamic model, the discharge and charge mode has been calculated to get the output voltage from the battery. The variables on equations 10 and 11 is explained in Nomenclature section. The simulation discharge curves for the Li-ion battery system (i.e. 48 V and 34 Ah) are shown in Figure 8. Some coefficients are calculated and known by the voltage and ampere-hour curve. This curve also represents the discharge behavior and the nominal area with exponential to better understand the harmless operating strategy to increase the lifetime of the battery.
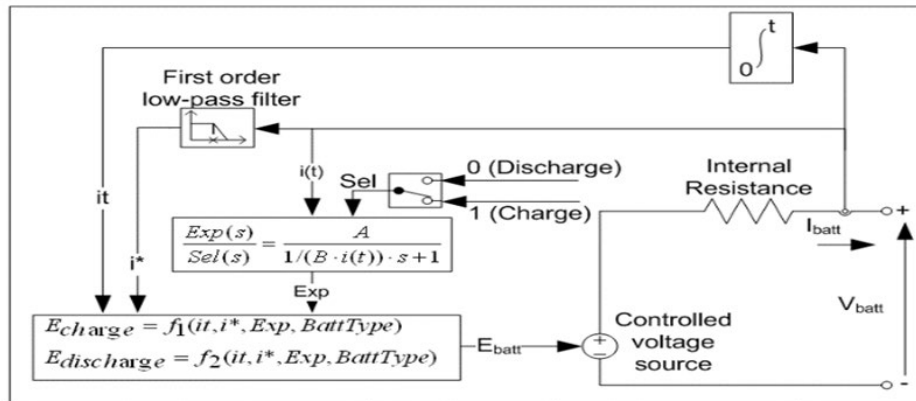

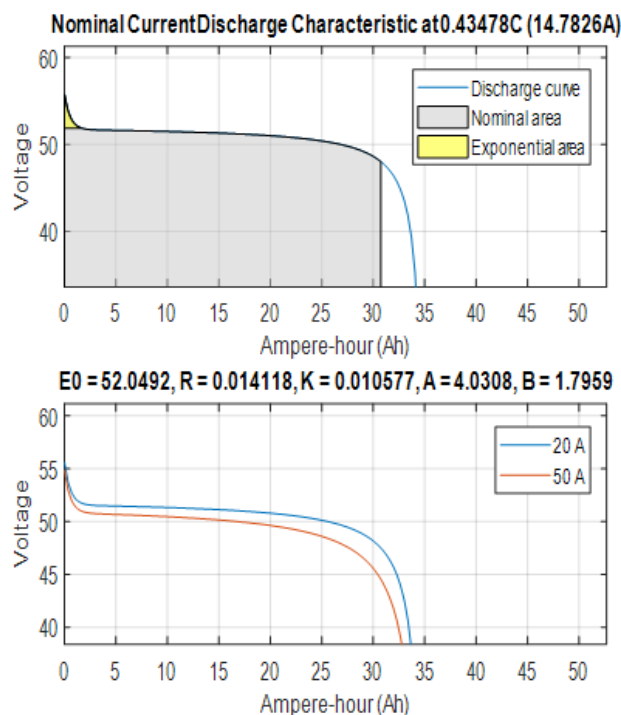**Figure 7.** Dynamic model for Li-ion battery [5].

Figure 8. Simulation discharge curves for the Li-ion battery [5].

2.4. Brushless DC motor

A brushless DC motor can be defined as a self-synchronous rotating motor, and it has a rotor with a permanent magnet [7]. To control the electronic commutation and rotor position signal, the commutation circuit on the ontology of the motor can be installed independently or integrated into it. The main components of the BLDC motor are the stator with its armature winding and the rotor with

a permanent magnet pole, which are very similar to the permanent magnet synchronous motor [7]. The electromagnetic torque model for the BLDC motor can be represented by equation 12, and the dynamic motion can be obtained by equation 13 [15].

$$T_e = \frac{1}{\omega_r}(e_a i_a + e_b i_b + e_c i_c) \tag{12}$$

$$\frac{d}{dt}\omega_r = \frac{1}{J} * (T_e + T_L + B\omega_r) \tag{13}$$

The MUN Explorer uses a propulsion system that has two standard blades (Wageningen B-series propeller type that is 0.65 m in diameter). A BLDC motor is used to drive the propulsion system. Figure 9 shows the schematic of the BLDC motor for the MUN Explorer. Table 2 shows the parameters of the BLDC motor, which is entered into the brushless DC motor in a MATLAB / Simulink block. These parameters are collected and verified from the MUN Explorer AUV data sheet.
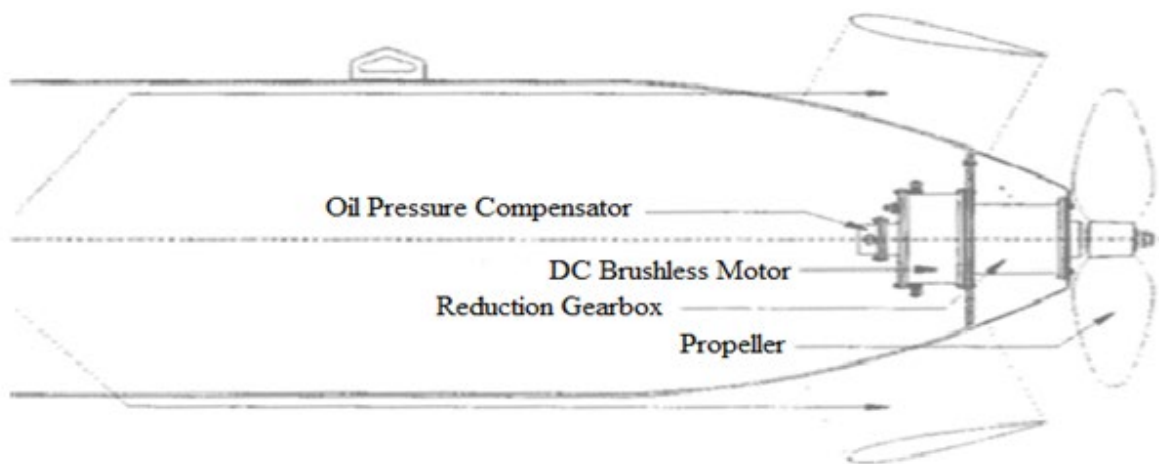

Figure 9. Schematic of the BLDC motor for the MUN Explorer.

Table 2. BLDC motor parameters.

Parameters	Value	Unit
Voltage	48	V
Resistance	0.2	Ohms
Inductance	8.5e-3	H
Friction Factor	0.005	N.m/A
Inertia J	0.089	Kg.m^2
Back EMF	120	Degrees

3. System control with a PI controller

The control system is important to maintain certain operating conditions such as controlling the motor speed, reducing the hydrogen gas consumption and improving the overall system efficiency. These conditions can be maintained by controlling the power outcome of the *PEM* fuel cell and the battery along the BLDC motor through the convertors using a PI controller.

In [4], the *PI* controller is implemented based on the battery SOC behavior, so the PI regulator

output is defined (in this case) as the battery power by removing it from the load power to get the fuel cell reference power. When the power of the fuel cell is reduced, the battery state of charge is above the reference value, which means the battery gives its full power. When the battery *SOC* is less than the reference value, the fuel cell delivers almost the load power. This controller can be tuned easily to get an acceptable response when compared to the other controller. The main function of this controller is to meet the parameters shown in Table 1. The dynamic model system using the PI controller is implemented and illustrated in MATLAB/Simulink as shown in Figure 10. The output from the PI controller is the maximum current of the fuel cell that is fed into the convertor to maintain 48 *VDC*. The two blue boxes are the minimum voltage (47.5 *V*) and the maximum voltage (52 *V*) to give the controller more fixability for maintaining the desired value (48 *VDC*).
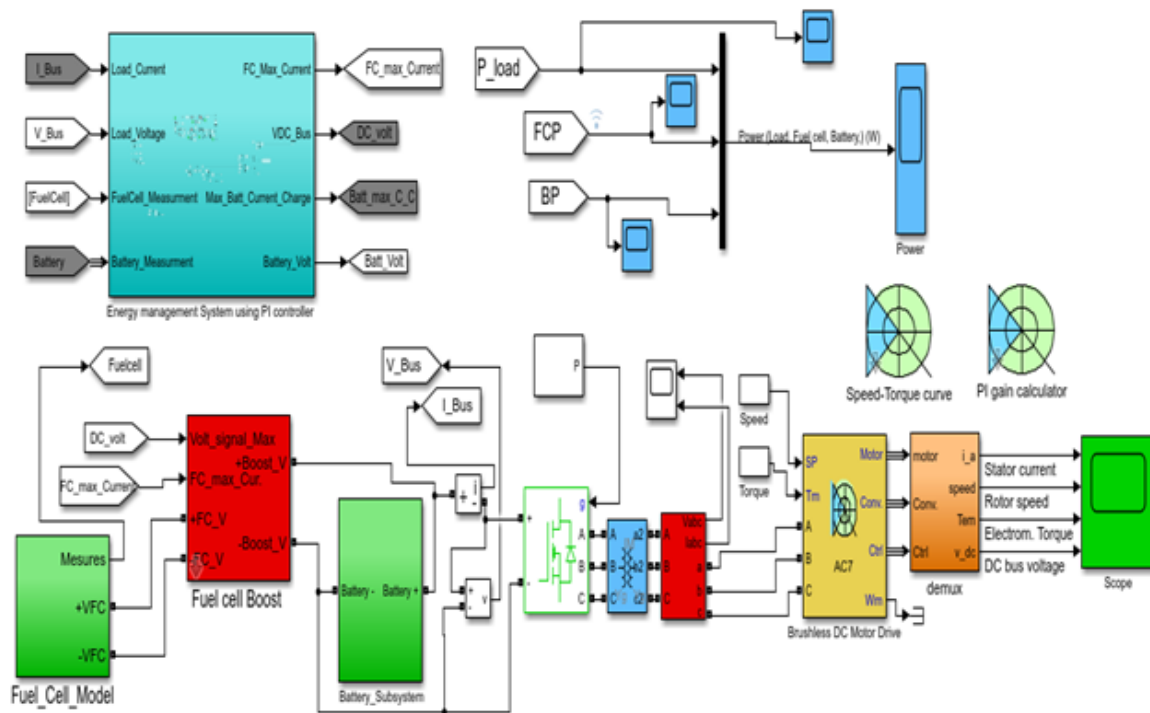

Figure 10. The PI controller for the maximum fuel cell current [4].

The minimum and maximum voltage value are representing the allowable voltage range to charge the battery with less harmful. If the battery exceeds these values, an explosion and damage can occur. Finally, in MATLAB / Simulink, the complete system was created and modified to show the dynamic model system using the PI controller, as shown in Figure 11. The main components of the system are the fuel cell system with oxygen and hydrogen tanks, a Li-ion battery, the BLDC motor and the energy management block, which controls the output parameters of each block and maintains the parameters shown in Table 1. The auxiliary components are boost converters, buck converters, the universal bridge, the speed-torque curve and the PI gain calculator.
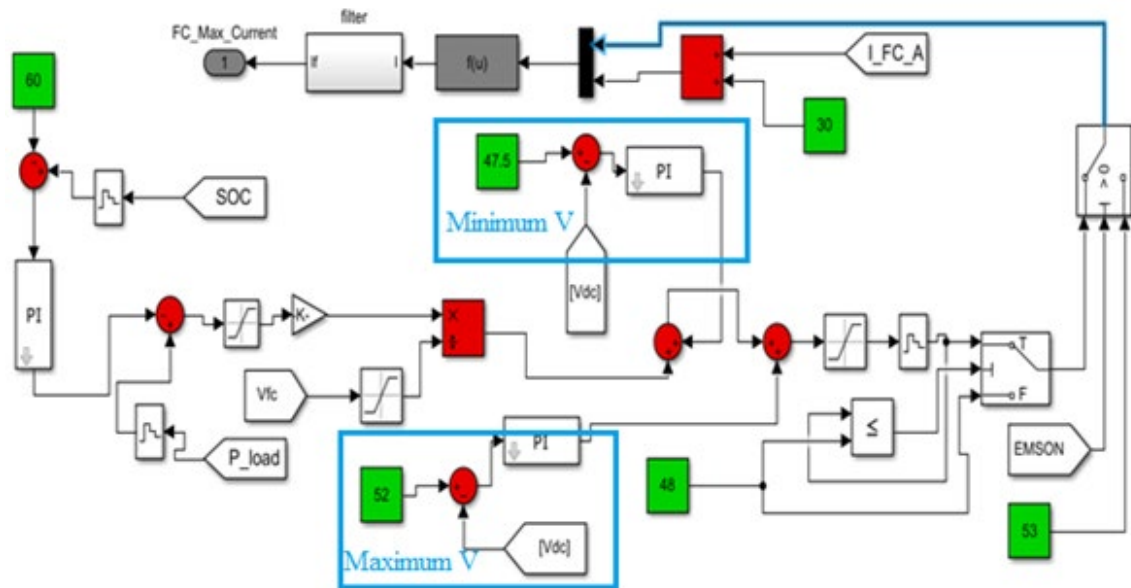
Figure 11. Complete system in MATLAB / Simulink.

4. Results and discussion

The integration of the fuel cell into the existing battery power system plays a significant role in running the MUN Explorer *AUV* under the desired and proper operating conditions.

To maintain these conditions, an energy management system using a PI controller has been implemented into the dynamic model of the MUN Explorer. Figure 11 explains the block connections of the complete model with the PI controller energy management system in MATLAB/Simulink. Figure 12 shows the relationship between the load torque and motor speed. This curve can be generated from Speed-Torque block in Figure 11. The Y-axis shows the load torque applied to the motor, and the X-axis represents the speed of the motor. The limits of the operating region illustrate the maximum load torque where the drive can maintain the desired speed at 20 (rad/s). The yellow region shows the load torque in acceleration, and the gray region illustrates the speed in steady-state operation. The BLDC motor was able to achieve the operating conditions by controlling the torque and speed and maintaining them at the desired points. The curve between the load torque and speed is plotted to get the idea of the operating point in the region. The input power of the BLDC motor is decreased when the power of the battery and fuel cell decreased too. Since the fuel cell and battery is directly connected to the BLDC motor, the dropping power is caused the mechanical output torque to decrease too. Since the stator current is proportional to the torque, the stator current is decreased as well. Also, the rotor speed is decreased when the input power goes down.

Figure 13 shows the simulation results for the stator current, rotor speed, electromagnetic torque and DC bus voltage. From the results, the stator current value is varying between 10 and −10 A, and the rotor speed (*wm*) is 20 rad/s, which is equivalent to 190 (*rpm)*. These values are verified and confirmed by the MUN Explorer manufacturer's data sheet. The electromagnetic torque (*Tem*) is also changing from (10 to −10) N-m. The DC bus voltage has 48 V, which verifies the motor drive voltage. Moreover, there is also a jump of the four physical quantities (stator current, rotor speed,

electromagnetic torque and DC bus voltage) due to the fuel cell dynamics and starting points. As noticed by the manufacture of the fuel, it takes up to 20 seconds to be turned on and generate the voltage.

The power profile for the load, fuel cell and the battery are illustrated in Figure 14. The blue result shows the load power (*W*), which represents the BLDC motor load. Similarly, the red and yellow results show the power profile (*W*) for the fuel cell and battery, respectively. The results illustrate that the fuel cell and battery power follow the load demand, and then the battery power decreases to let the fuel cell generate the maximum power.

Each power profile is plotted in a separate figure that can be seen in the appendix. From the figures, the changing in the power profile between 20 sec to 30 sec is caused by the fuel cell starting operating points due to the dynamic characteristic behavior.

The simulation runs for 100 (seconds) to ensure the values of Table 1 are met and verified. It should have been run for 3600 seconds (1 hr) or at least 1800 seconds (30 min), but the lack of memory prevents it from achieving these times. Figure 15 shows the three-phase voltage and current measurements of the model. As seen in Figure 15, the results show good agreement in terms of voltage and current measurements.

The hydrogen fuel consumption is illustrated in Figure 16. It shows the fuel consumption increase over time. To meet the proposed values in Table 1, the control system using the PI controller is implemented and studied. The classical PI control results show that the battery discharges faster in order to get the SOC reference point, whereas the fuel cell provides almost all the load power and recharges the battery. The PI controller provides a good result to meet the power requirements, but these results can be improved by implementing a different controller such as a Fuzzy-Logic Controller (*FLC*). An *FLC* will give better results as suggested in the literature.
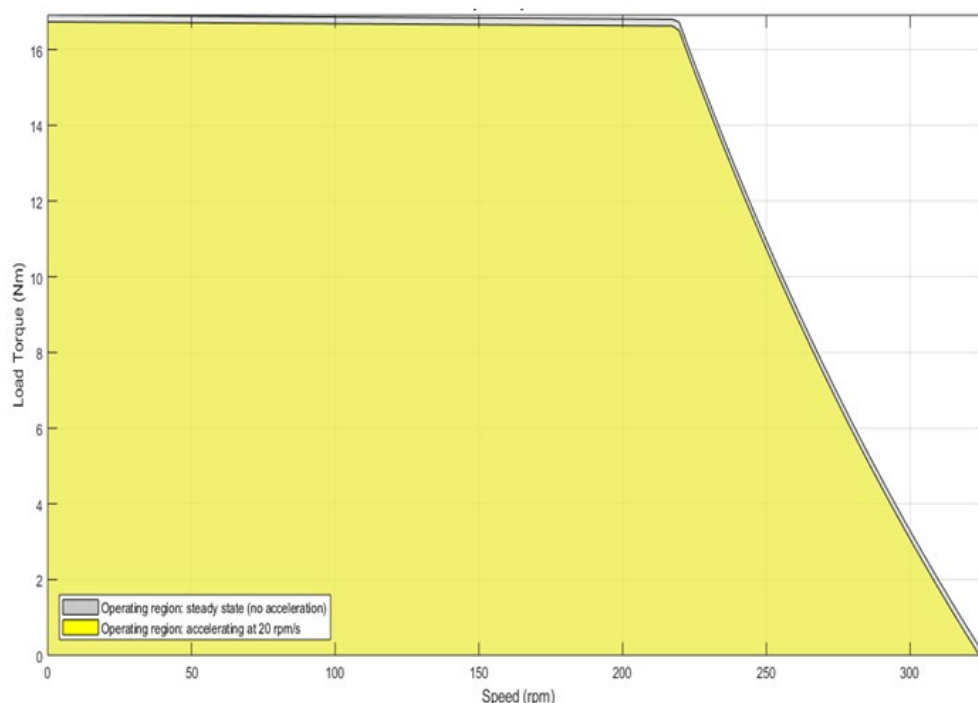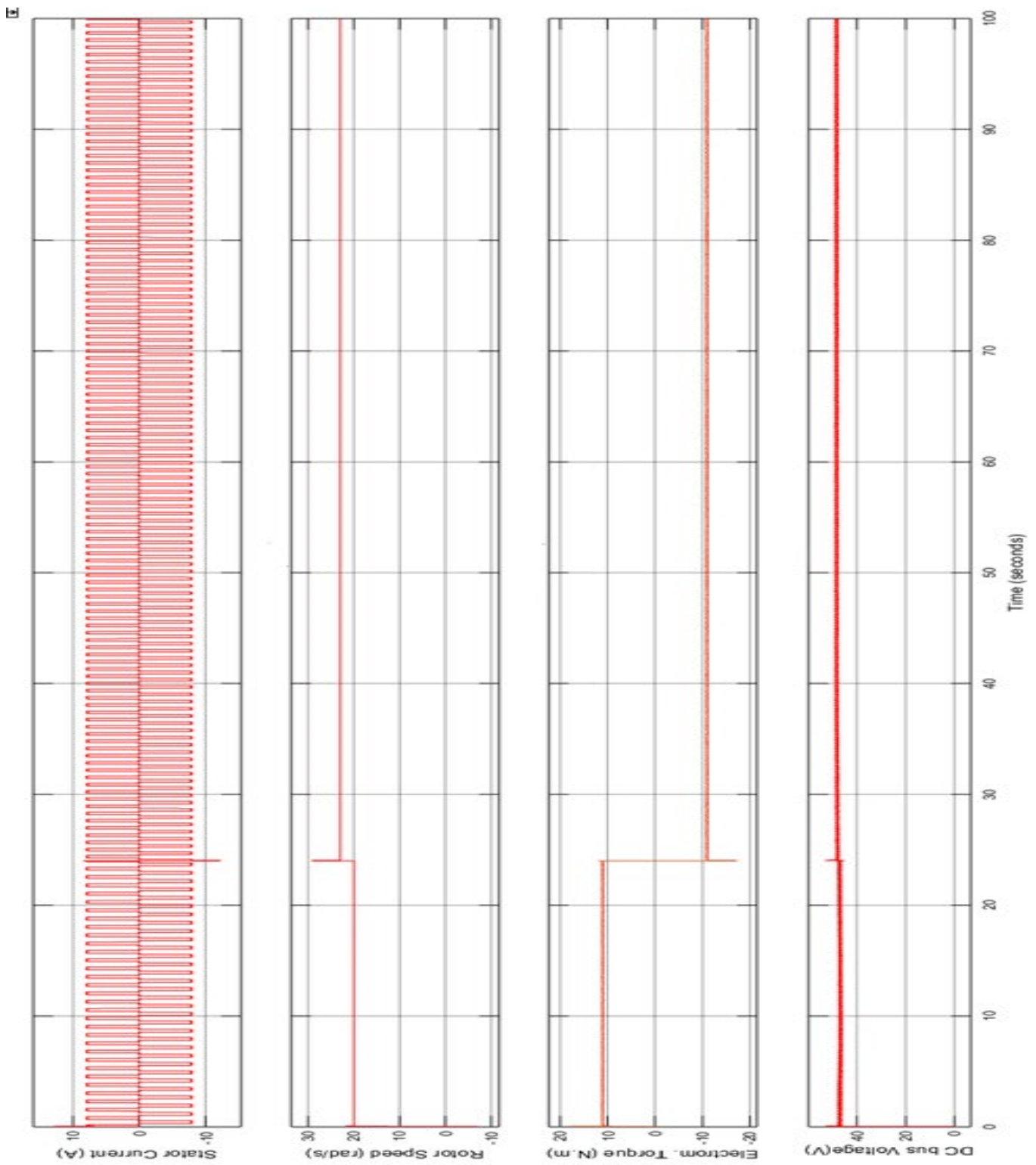

Figure 12. Load torque versus speed motor.

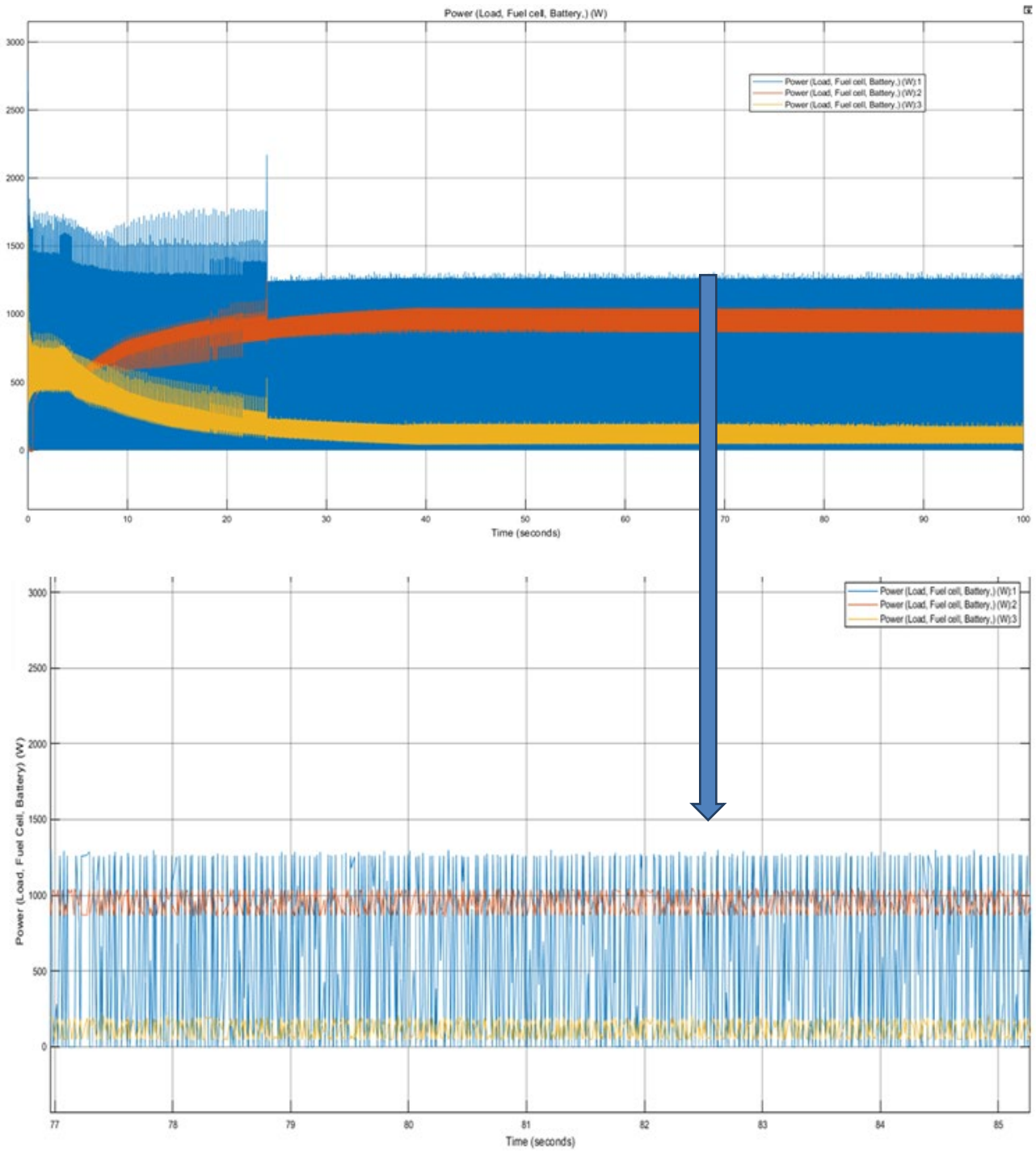**Figure 13**. Simulation results for stator current, rotor speed, electromagnetic torque and DC bus voltage.

Figure 14. Power profile for the load, fuel cell and the battery in (W).
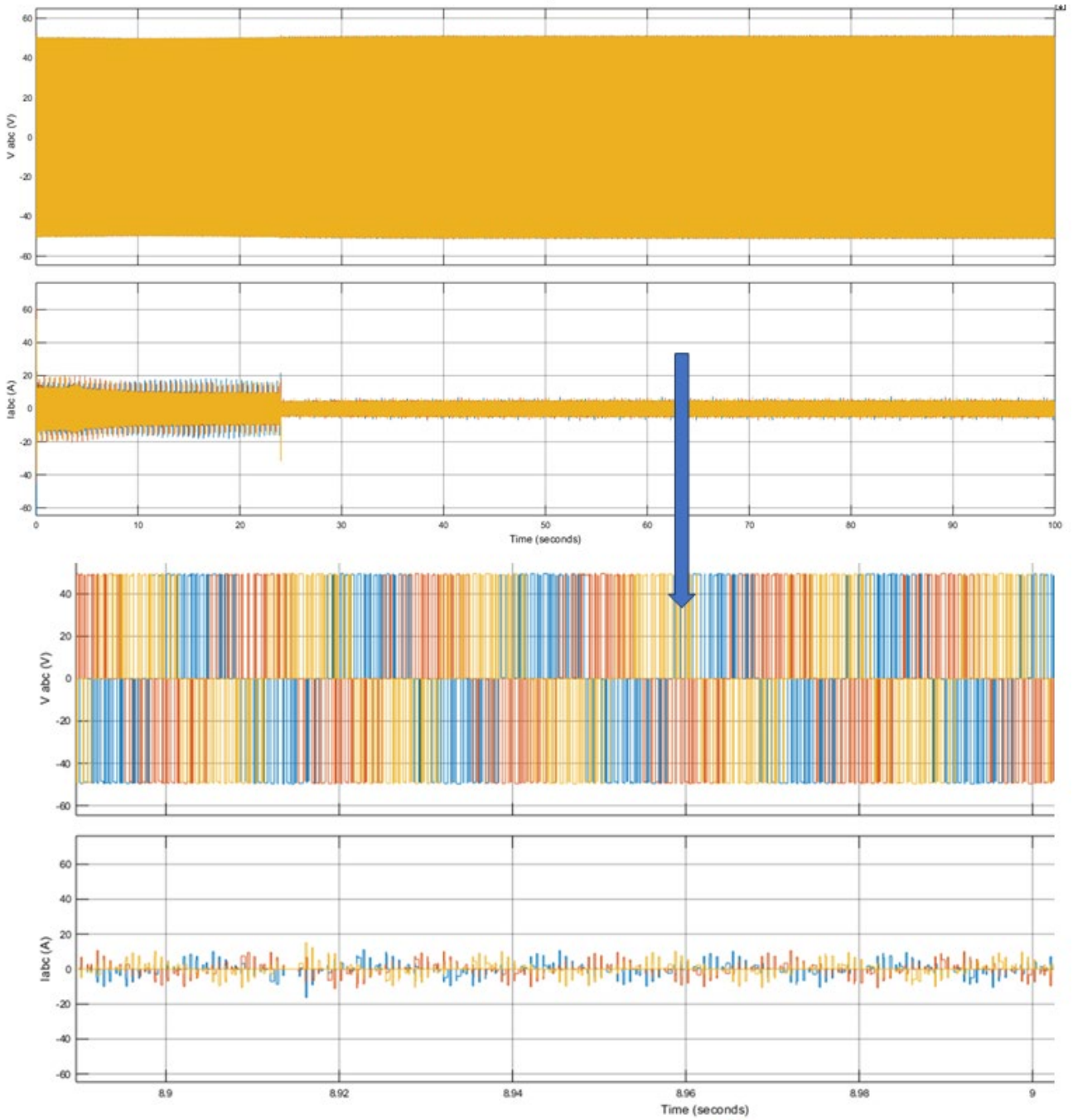
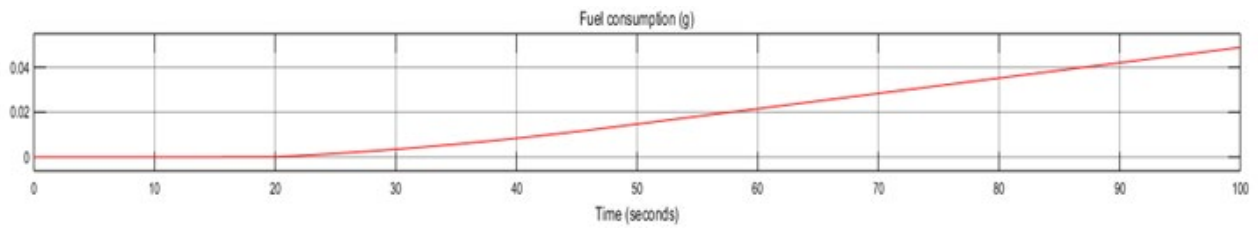**Figure 15**. Three-phase voltage and current measurements.

Figure 16. Hydrogen fuel consumption (g).

5. Conclusion

The control system using a *PI* controller for the MUN Explorer Autonomous Underwater Vehicle's power system was studied and implemented in this paper. To ensure that the MUN Explorer runs efficiently and smoothly, some power requirements were imposed and studied as shown in Table 1. The power profile for the fuel cell and battery were presented and discussed as well as the power load profile. All the data for the *BLDC* motor and battery were collected and applied from the manufacturer's data sheet to meet the exact same operating conditions. The *PI* controller showed good results in terms of the response. The *DC* bus voltage was measured at 48 *V*, and the motor speed was 20 (*rad/s*), which is equivalent to 190 (*rpm*). The system components were simulated in MATLAB / Simulink. The *PI* controller is a simple controller to be implemented into the proposed system and to tuned easily.

Future work that builds on this research should implement other types of controllers such as Fuzzy logic controllers or state machine controllers. A Fuzzy controller would be the best choice for such a system. Other future work could be done to experiment with this model to verify the simulation results.

Acknowledgements

Conflict of interest

The authors declare that there is no conflict of interest regarding to this publication.

References

1. Cirrincione M, Cossentino M, Gaglio S, et al. (2009) Intelligent energy management system. *IEEE Int Conf Ind Informatics* 232–237.
2. Barchi G, Miori G, Moser D, et al. (2018) A Small-Scale Prototype for the Optimization of PV Generation and Battery Storage through the Use of a Building Energy Management System. *2018 IEEE International Conference on Environment and Electrical Engineering and 2018 IEEE Industrial and Commercial Power Systems Europe (EEEIC / I&CPS Europe)*.
3. Kumaraswamy VK and Quaicoe JE (2016) Tracking techniques for the PEMFC in portable applications. *2016 IEEE Electrical Power and Energy Conference (EPEC)*.
4. Motapon SN, Dessaint LA, Al-Haddad K (2014) A comparative study of energy management schemes for a fuel-cell hybrid emergency power system of more-electric aircraft. *IEEE T Ind Electron* 61: 1320–1334.
5. Albarghot MM, Iqbal MT, Pope K, et al. (2019) Sizing and Dynamic Modeling of a Power System for the MUN Explorer Autonomous Underwater Vehicle Using a Fuel Cell and Batteries. *J Energy* 2019: 4531497.
6. Motapon SN, Lupien-Bedard A, Dessaint LA, et al. (2017) A Generic Electrothermal Li-ion Battery Model for Rapid Evaluation of Cell Temperature Temporal Evolution. *IEEE T Ind Electron* 64: 998–1008.

7. Xie W, Wang JS, Wang HB (2019) PI Controller of Speed Regulation of Brushless DC Motor Based on Particle Swarm Optimization Algorithm with Improved Inertia Weights. *Math Probl Eng* 2019: 1–12.

8. Wang Y, Sun Z, Chen Z (2019) Development of energy management system based on a rule-based power distribution strategy for hybrid power sources. *Energy* 175: 1055–1066.

9. Wang Y, Sun Z, Chen Z (2019) Energy management strategy for battery/supercapacitor/fuel cell hybrid source vehicles based on finite state machine. *Appl Energy* 254: 113707.

10. Wang Y, Sun Z, Li X, et al. (2019) A comparative study of power allocation strategies used in fuel cell and ultracapacitor hybrid systems. *Energy* 189: 116142.

11. Wang Y, Li X, Wang L, et al. (2019) Multiple-grained velocity prediction and energy management strategy for hybrid propulsion systems. *J Energy Storage* 26: 100950.

12. Görgün H (2006) Dynamic modelling of a proton exchange membrane (PEM) electrolyzer. *Int J Hydrogen Energy* 31: 29–38.

13. Rigatos G and Siano P (2016) A PEM fuel cells control approach based on differential flatness theory. *2016 International Symposium on Power Electronics, Electrical Drives, Automation and Motion (SPEEDAM)* 2: 1004–1009.

14. Souleman NM, Tremblay O, Dessaint LA (2009) A generic fuel cell model for the simulation of fuel cell vehicles. *2009 IEEE Vehicles Power and Propulsion Conference* 1722–1729.

15. Geraee S, Shafiei M, Sahami AR, et al. (2017) Position sensorless and adaptive speed design for controlling brushless DC motor drives. *2017 North American Power Symposium NAPS*.

Appendix

A. Propulsion system

A.1. Motor

Manufacturer	Hathaway Emoteq, Inc
Model	HT07001-H01
Design voltage (V) DC	48
Maximum current (Amp) (input to motor controller)	32
Maximum PRM in water – @ 2.5 m/s	300
Maximum PRM (W) (input to motor controller)	1630@51 VDC

A.2. Motor controller

Manufacturer	Hathaway Emoteq, Inc
Model	B2Q04840
Peak current (Amp) (Output of motor controller)	40
Minimum D. C. supply (V)	40
Maximum D.C. supply (V)	60